

## Articles

---

### GRID/GOLPE 3D Quantitative Structure–Activity Relationship Study on a Set of Benzamides and Naphthamides, with Affinity for the Dopamine D<sub>3</sub> Receptor Subtype

Jonas Nilsson\* and Håkan Wikström

*Department of Medicinal Chemistry, University Centre for Pharmacy, Antonius Deusinglaan 1, NL-9713 AV Groningen, The Netherlands*

Age Smilde

*Laboratory for Analytical Chemistry, University of Amsterdam, Nieuwe Achtergracht 166, NL-1018 WV Amsterdam, The Netherlands*

Shelly Glase and Tom Pugsley

*Departments of Chemistry and Therapeutics, Parke-Davis Pharmaceutical Research Division, Warner-Lambert Company, 2800 Plymouth Road, Ann Arbor, Michigan 48105*

Gabriele Cruciani, Manuel Pastor, and Sergio Clementi

*Department of Chemistry, University of Perugia, Via Elce di Sotto, 10, 06123 Perugia, Italy*

Received August 19, 1996<sup>⊗</sup>

In the search for drugs against schizophrenia and depression without extrapyramidal side effects, compounds that selectively antagonize the dopamine D<sub>3</sub> receptor subtype are thought to be a solution. In order to create a model with which the D<sub>3</sub> activity can be predicted and that can generate new ideas for future synthesis, we performed a comparative molecular field analysis (CoMFA). In our model 30 ligands were described quantitatively in the GRID program, and the model was optimized by selecting only the most informative variables in the GOLPE program. We found the predictive ability of the model to increase significantly when the number of variables was reduced from 25 110 to 784. A  $Q^2$  of 0.65 was obtained with the final model, confirming the predictive ability of the model. By studying the PLS coefficients in informative 3D contour plots, ideas for the synthesis of new compounds can be generated.

#### Introduction

The dopamine D<sub>3</sub> receptor is characterized by its selective expression in mesolimbic dopaminergic projection areas of the rat and human brains and its high affinity for antipsychotic drugs, suggesting a role of its receptor in the control of locomotion and motivation, as well as in the pathogenesis of disorders such as drug abuse and schizophrenia.<sup>1</sup> Existing drugs against schizophrenia cause major movement disorders called extrapyramidal syndrome (EPS), proposed to be caused by blockade of D<sub>2</sub> receptors in the striatum. The 30 ligands<sup>2</sup> included in this study were synthesized with the aim to achieve ligands that selectively could antagonize the D<sub>3</sub> receptor and thereby also avoid the EPS. The ligands belong to two different classes, benzamides and naphthamides, both having an arylpiperazine tail connected to the amide nitrogen. We wanted to create a model, including those ligands, able to predict the activities of compounds not yet synthesized and that could serve as a help in the design of new compounds. Traditionally, SYBYL/CoMFA<sup>3,4</sup> (comparative molecular field analysis) is the method used to create this kind of models, but there are other 3D QSAR (quantitative

structure–activity relationship) methods available<sup>5,6</sup>. We decided to use the GRID program<sup>6</sup> to generate molecular descriptors and the GOLPE program<sup>5</sup> for the multivariate regression analyses.

#### Theory and Methods

**Computer Hardware.** All calculations presented were carried out on a R4600 Indy Silicon Graphics workstation.

**Molecular Descriptors Generated in the GRID Program.** In both SYBYL/CoMFA<sup>4</sup> and GRID,<sup>6</sup> a grid, big enough to enclose all the aligned ligands in all directions, is created. Subsequently, interaction energies between a probe atom and the target molecule are calculated, in each grid point. However, SYBYL/CoMFA and GRID use different force fields and different types of probe atoms, and as a consequence, the results will differ. Interactions recognized and accounted for in the GRID force field are steric, electrostatic, and hydrogen-bonding interactions represented by the Lennard–Jones energy ( $E_{STE}$ ), the Coloumbic energy ( $E_{EL}$ ), and a hydrogen-bonding ( $E_{HB}$ ) term, respectively. In contrast to SYBYL/CoMFA, where all interaction energies are considered separately, the sum of all the different interaction energies (eq 1) is calculated in the GRID program. An attractive interaction yields a negative field ( $E_{xyz}$ ), while repulsive interactions are positive.

$$E_{xyz} = E_{EL} + E_{STE} + E_{HB} \quad (1)$$

Different probes reflect different types of interactions and may

\* Author to whom correspondence should be addressed.

⊗ Abstract published in *Advance ACS Abstracts*, February 1, 1997.

selectively be included to mimic specific interactions between the ligand and the receptor. Often more than one probe is necessary for a complete description of the different interaction types.

**Data Pretreatment.** The outcome of a CoMFA is dependent on the pretreatment of the initial quantitative descriptors,<sup>7</sup> that is, mathematical manipulations performed in order to minimize the influence of insignificant variation, on the final model. GOLPE offers a number of different options for pretreatment and may be used in combinations, or not at all, depending on the heritage of the data we are working with.

A probe too close to the target molecule may produce unrealistic high-positive (repulsive) interactions that can influence the PLS solution detrimentally. Therefore, it is wise to introduce a positive maximum cutoff value. The negative interaction values (attractions) decline smoothly as the distance between the probe and the target molecule increases, and a cutoff value for negative values is not necessary.

Interaction values in grid points in the periphery of the grid tend to be low, where variations are more similar to noise than true reflections of the variations in the field. The zeroing option corrects for this by replacing absolute values, lower than a specified cutoff value, with zero.

Grid points with a too low standard deviation may be assessed insignificant and consequently be omitted from the analysis. This option is identical with the "MINIMUM\_SIGMA" option in SYBYL/CoMFA.

In some grid points it is possible that all ligands but one have identical interaction values (e.g., maximum cutoff), and consequently, PLS adjusts its solution for this single variable.<sup>5</sup> These types of variables, called 2-level variables, may produce spurious PLS solutions and can optionally be omitted with a more stable PLS model as a result. Similarly, also 3- and 4-level variables can be omitted.

Finally, traditional autoscaling is also an option, but for data of the GRID type a more suitable pretreatment is the block-scaling option. In autoscaling, the sum of squares within each variable is equalized or, more simply, the standard deviation of each variable is normalized. In block-scaling, the sum of squares within each grid (i.e., interaction values from each probe) is normalized. This is identical with the "CoMFA\_std" scaling option in SYBYL/CoMFA.

**Statistical Tools.** In order to compare the performance of the different models, multivariate tools are needed. In 3D QSAR data, severe variance between variables disqualifies multiple-linear regression (MLR)<sup>8</sup> as the regression method, and another method is needed. PLS (partial least squares)<sup>8,9</sup> is the multivariate regression method implemented in most QSAR software packages,<sup>3</sup> which is a least-squares regression method working not on the original variables but instead on underlying latent variables. Covariance in the data reduces the number of significant latent variables and thereby also the complexity of the model. A more detailed description of the PLS algorithm is presented by Geladi et al.<sup>8</sup>

The multivariate analogue to the univariate correlation coefficient ( $r^2$ ) is the fitted  $R^2$  calculated as in eq 2, used to evaluate whether the data are correlated or not.

$$R^2 = 1 - \frac{\sum_i (y_{\text{calc}} - y_{\text{obs}})^2}{\sum_i (y_{\text{obs}} - y_{\text{mean}})^2} \quad (2)$$

The  $R^2$  explains the fraction of the total variation, in  $y$ , accounted for by the model, and consequently, a model with perfect correlated data has a  $R^2$  of 1.

In 3D QSAR, where highly predicted models are desired, cross-validation<sup>10</sup> is used as an internal measure of the predictive ability. In cross-validation, a model is calculated with a group of objects omitted subsequently followed by prediction of the omitted objects, and the procedure is repeated until all objects have been omitted once. A model with low prediction errors will have a  $Q^2$  (eq 3) close to 1, while a model with negative  $Q^2$  will predict no better than random.

$$Q^2 = 1 - \frac{\sum_i (y_{\text{ipred}} - y_{\text{obs}})^2}{\sum_i (y_{\text{obs}} - y_{\text{mean}})^2} \quad (3)$$

$Q^2$  is frequently used in 3D QSAR, and recently also the SDEP (standard deviation error of predictions, eq 4) was suggested.<sup>11</sup> The SDEP has the advantage of having the same unity as the dependent variable ( $y$ ) and, according to the authors, is therefore more informative than the  $Q^2$ .

$$\text{SDEP} = \left[ \sum_i (y_{\text{ipred}} - y_{\text{obs}})^2 / N \right]^{1/2} \quad (4)$$

**D-Optimal Preselection of Variables.** D-Optimal<sup>12,13</sup> preselection of variables and variable selection guided by a fractional factorial design (FFD) form the basis of the GOLPE algorithm (generating optimal linear PLS estimations).<sup>14</sup>

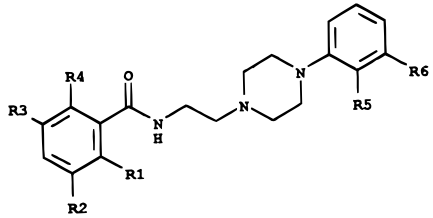
The data generated in GRID contains a large number of variables, and still, after pretreatment, only a fraction of them contains information correlated with the biological activity ( $^{10}\log K_i$ ). In GOLPE, only the most informative variables are selected by a D-optimal preselection from an initial PLS model. (The dimensionality of the PLS model is determined by cross-validation.<sup>10</sup>) Roughly speaking, variables are selected to span the multidimensional weight space, in the best way possible. The selection procedure is iterative, and after each selection a new PLS model is calculated including only the selected variables. The selection procedure is repeated until the fitted  $R^2$  starts to decrease. Baroni et al.<sup>14</sup> suggest not more than 50% of the variables should be omitted each time. During the preparation of this work, we learned that the D-optimal preselection procedure may be used to reduce the number of variables from, roughly, tens of thousands to thousands of variables before the fitted  $R^2$  starts to decrease.

**Variable Selection following a Fractional Factorial Design (FFD) Procedure.** At this point, most of the redundant variables have been eliminated, and the predictability of the model, in terms of predicted  $Q^2$ , can be optimized. The influence of each variable on the predictive ability is estimated by a number of cross-validation experiments where variables are included and excluded, alternately. A design matrix,<sup>14</sup> with a number of columns equal to the number of variables left after the D-optimal preselection and with 2 times as many rows, is created. Each row represents an experiment where "plus" and "minus" signs mean include and exclude a variable in the experiment, respectively. Obviously, different combinations of variables generate different SDEP, and by means of Yates' algorithm,<sup>15</sup> the influence of each individual variable on the SDEP can be calculated. In order to separate a variable that significantly improves predictability from one that does not, a number of variables with random numbers are introduced in the design matrix. A random variable has, by definition, no influence on the predictability of the model. Therefore, the estimated average effect of the random variables may serve as a limit, on the basis of a Student's  $t$ -test at the 95% confidence level, for the estimated effects of the true variables. A true variable with a significantly higher estimated effect than the limit will be excluded. A true variable with a significantly lower estimated effect than the limit will be kept fixed, and a true variable with an estimated effect within the limit interval may optionally be fixed or excluded.

The coordinates of the ligands included in this work are available from the author upon request (e-mail: j.nilsson@farm.rug.nl).

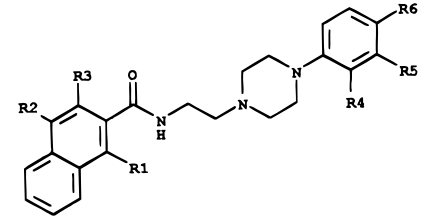
## Results and Discussion

**Molecular Modeling.** Initially, 30 molecules (Tables 1–3) were built and minimized using the MM2\* force field implemented in the molecular modeling package Macromodel 4.5.<sup>16</sup> In order to simplify the calculations, two general assumptions concerning the conformations were made. First, the benzamide part of the ligands was fixed in a planar conformation ( $\tau(5-6-7-8)$  in Figure 1 set to  $0^\circ$ ), as supported from several X-ray structures present in the Cambridge Crystallographic Structural Database (CSD). Additionally, the oxygen from the *o*-methoxy (Figure 1, atom 5) stabilizes the

**Table 1.** Benzamide Ligands and Their Experimental and Calculated Affinities for the Dopamine D<sub>3</sub> Receptor Subtype


compd	R1	R2	R3	R4	R5	R6	<sup>10</sup> log K <sub>i</sub> (nM)	
							expt <sup>a</sup>	calcd
1	-OMe		-Br				2.5	2.6
2	-OMe		-Br	-OH			2.6	2.8
3	-OMe	-Et	-Cl	-OH			3.2	3.1
4	-OMe	-Cl	-Cl	-OH			3.0	2.9
5	-OMe	-Cl	-Cl	-OH	-Cl	-Cl	2.7	2.7

<sup>a</sup>[<sup>3</sup>H]Spiperone, human DA D<sub>3</sub> receptors expressed in CHO K1 cells; K<sub>i</sub> values were obtained from four to six concentrations, run in triplicate, by a nonlinear regression analysis.

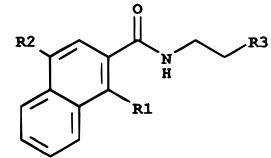
**Table 2.** Naphthamide Ligands and Their Experimental and Calculated Affinities for the Dopamine D<sub>3</sub> Receptor Subtype


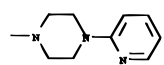
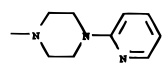
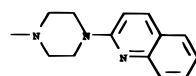
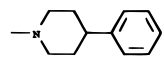
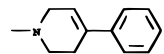
compd	R1	R2	R3	R4	R5	R6	<sup>10</sup> log K <sub>i</sub> (nM)	
							expt <sup>a</sup>	calcd
6	-OMe	-Br					1.4	1.9
7	-OMe	-Cl					1.7	1.9
8	-OEt	-Br					2.4	2.0
9	-OMe	-Br		-OMe			1.9	1.7
10	-OEt	-Br		-OMe			1.9	1.8
11		-Br	-OMe				2.5	2.3
12	-OMe	-Br			-CF <sub>3</sub>		2.4	2.2
13	-OEt	-Br			-CF <sub>3</sub>		2.1	2.3
14	-OMe	-Br		-CN			1.7	1.5
15	-OMe	-Br		-Me			1.8	1.6
16	-OMe	-Br			-Me		2.5	2.2
17	-OMe	-Br				-Me	2.4	2.3
18	-OMe	-Br		-Me	-Me		1.7	1.7
19	-OMe	-Br		-Cl			1.6	1.5
20	-OMe	-Br			-Cl		1.6	2.0
21	-OMe	-Br			-Cl	-Cl	2.3	2.4
22	-OMe	-Br		-Cl	-Cl	-Cl	2.0	2.0
23	-OMe	-Cl		-Cl	-Cl		1.6	1.7
24	-OMe	-Br		-F		-F	2.3	2.0
25	-OMe	-Br		-Me	-Cl		1.7	1.7

<sup>a</sup>[<sup>3</sup>H]Spiperone, human DA D<sub>3</sub> receptors expressed in CHO K1 cells; K<sub>i</sub> values were obtained from four to six concentrations, run in triplicate, by a nonlinear regression analysis.

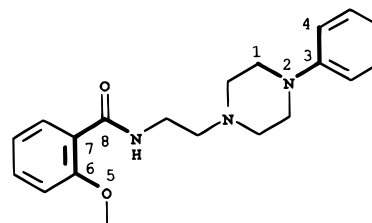
conjugated benzamide part by forming an internal hydrogen bond with the amide N-H.

The second assumption concerns the arylpiperazine tail, the conformation of which we also fixed with support from X-ray structures. The piperazine ring in a chair conformation was present in all arylpiperazines found in CSD, suggesting that this conformation is energetically preferable, as compared to the boat conformation. A conformational search experiment in SYBYL (Tripos force field<sup>17</sup>) confirmed this, by finding the chair conformation in all low-energy conformations (not presented). The torsional angle between the piperazine ring and the phenyl ring (Figure 1,  $\tau(1-2-3-4)$ ), however, was more flexible. An unsubstituted

**Table 3.** Additional Naphthamide Ligands and Their Experimental and Calculated Affinities for the Dopamine D<sub>3</sub> Receptor Subtype


Comp.	R1	R2	R3	<sup>10</sup> log K <sub>i</sub> <sup>a</sup> (nM) exp.	<sup>10</sup> log K <sub>i</sub> (nM) calc.
26	-OMe	-Br		1.9	1.9
27	-OEt	-Br		1.9	2.0
28	-OMe	-Br		2.4	2.5
29	-OMe	-Br		1.9	1.8
30	-OMe	-Br		1.3	1.7

<sup>a</sup>[<sup>3</sup>H]Spiperone, human DA D<sub>3</sub> receptors expressed in CHO K1 cells; K<sub>i</sub> values were obtained from four to six concentrations, run in triplicate, by a nonlinear regression analysis.

**Figure 1.** Benzamide-phenylpiperazine skeleton. In order to simplify the modeling procedure, the highlighted torsional angles  $\tau(1-2-3-4)$  and  $\tau(5-6-7-8)$  were fixed at 84° and 0°, respectively, with support from X-ray structures.

phenyl ring can, according to X-ray structures, be found in almost any angle, while an ortho-substituted phenyl ring is more or less always somewhat twisted. Due to these findings we chose to fix the  $\tau(1-2-3-4)$  between the piperazine ring and the phenyl ring at 84°. As a consequence, the overlap of the phenyl rings from compound 30 (Table 3) and the rest of the ligands was improved.

The conformational space, of all ligands, was explored by a conformational search procedure using the Monte Carlo procedure, as implemented in Macromodel while keeping the above-discussed torsional angles fixed. New conformations were randomly generated, and their energy was minimized and subsequently compared with previously saved conformations. If a new conformation was lower in energy than the present "global minimum energy conformation", the new conformation replaced the old one. If a new conformation was identical with the global minimum energy conformation, a variable was increased by one, and when this conformation was found a sufficient number of times, the conformational search was considered converged. All conformations within 5 kcal/mol from the global minimum energy

**Table 4.** Description of the Eight Different Probes from Grid<sup>a</sup>

probe	description	probe	description
H	hydrogen atom	OH	OH with acidic H
<b>C3</b>	<b>sp<sup>3</sup> C atom</b>	<b>OH2</b>	<b>water</b>
O::	sp <sup>2</sup> O in C=O	NA+	sodium cation
O1	sp <sup>3</sup> O in O-H	<b>CA+1</b>	<b>calcium cation</b>

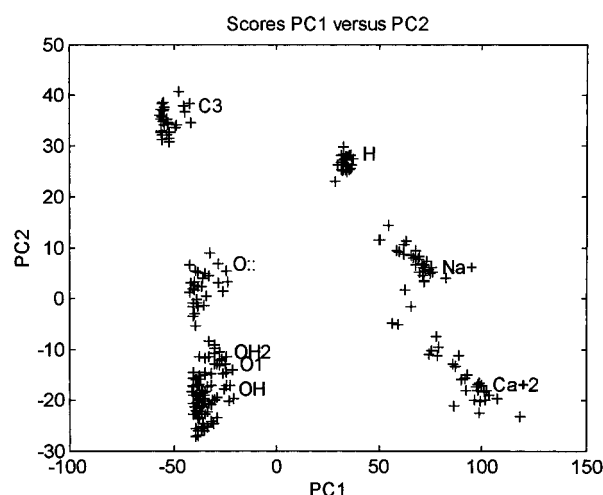
<sup>a</sup> The three selected probes are marked in bold face.

conformation were saved and considered as even likely to be the conformation interacting with the receptor.

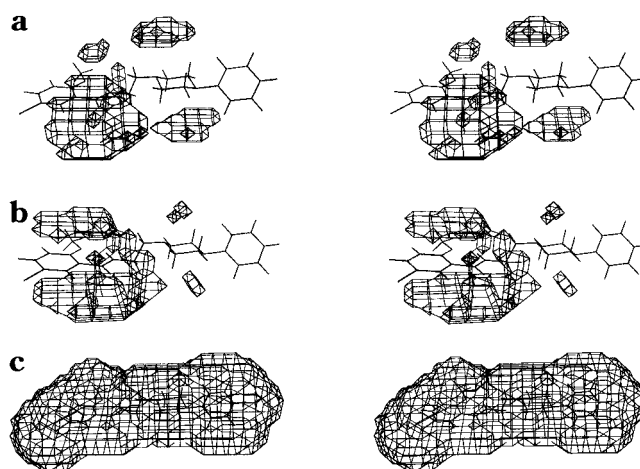
The most crucial step when preparing a CoMFA study is the alignment of the ligands. Since the homology between the ligands in the model is very high, the main goal with the alignment procedure was to achieve maximum overlap between the ligands. The pharmacophore, below, was chosen with this in mind. The midpoint of the aromatic benzamide ring, amide O, amide N-H, and a dummy atom in the direction of the lone pair of electrons from the basic nitrogen of the arylpiperazine part were identified as possible interaction points with the receptor. Dummy vectors and midpoints were added to each conformation from all ligands using vecadd, a subprogram in the pharmacophoric program Apollo.<sup>18</sup> Due to lack of a rigid template, the global minimum energy conformation from ligand **1** (Table 1) was chosen as template, and subsequently, all the other ligands were fitted on this template, on the pharmacophoric points identified above, using Apollo. Each fitting procedure considered all conformations within 5 kcal/mol from the global minimum as determined by the conformational search procedure. The output was a number of fits ranked in decreasing order of rms (root mean square). Optionally, the energy of a fitted conformation can be selected to affect the ranking, and consequently, the lower the energy of a fitting conformation the higher the rank of the fit becomes. The highest ranked conformation, from each ligand, was included in the final model. The selected ligands were converted into the Tripos mol2 format using the file-converting program Babel.<sup>19</sup>

**Receptor Binding.** The ligands' *in vitro* affinity for the human dopamine D<sub>3</sub> receptor subtype was the dependent variable considered in this study. In the antagonist binding study, the affinity of the compounds was determined by their ability to displace [<sup>3</sup>H]spiperone from the dopamine D<sub>3</sub> receptor.<sup>20</sup> Receptor binding affinities are mostly expressed as K<sub>i</sub> (nM) values calculated from IC<sub>50</sub> values as described by Cheng and Prusoff.<sup>21</sup> In order to get a more homogenous distribution of the dependent variable, we used the <sup>10</sup>log K<sub>i</sub> and, as a consequence, improved the result of the regression analyses.

**Probe Selection.** The grid created in GRID enclosed all the aligned ligands with 4 Å with a resolution of 1 Å in all directions. Consequently, the grid consisted of 8370 grid points, and interactions between all eight probes (Table 4) and all 30 ligands were calculated in each grid point, yielding a 240 × 8370 matrix. Subsequently, a principal component analysis (PCA)<sup>5,8,22</sup> was performed, where the first two components were sufficient to separate and identify clusters of ligands from the different probes. It can be concluded in the score plot (Figure 2) from the first two components that the CA+2, the C3, and the OH2 probes contained the most different information, and these were therefore selected. Interestingly, the O1, the OH, and the OH2 probes were



**Figure 2.** Plot of the scores from the first two components explaining 64% of the variation in the data matrix. Six obvious clusters can be recognized, and the three most different probes (C3, OH2, and CA+2) were selected for further modeling.

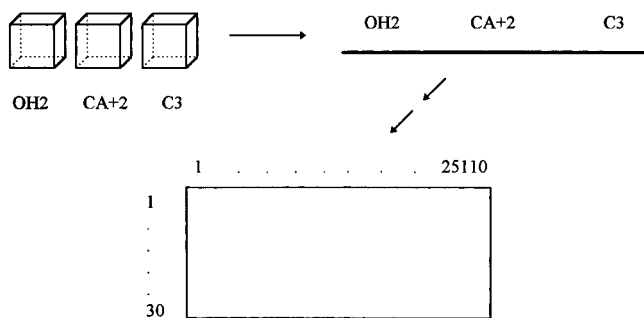


**Figure 3.** Contour maps of the actual OH2, CA+2, and C3 fields from molecule **1** on the  $-2.6$ ,  $-3.0$ , and  $0.02$  kcal/mol level, respectively: (a and b) regions where hydrogen bonds are favorable and where the CA+2 probe produces an attractive field with the molecule, respectively; (c) the C3 probe produces a repulsive field inside the region.

not possible to separate in the score plot, indicating that no extra information would be added to the model if more than one of them were included. Therefore, only the OH2 probe was selected.

Hydrogen bonding is one of the important interactions in the ligand–receptor interaction.<sup>6,23</sup> Figure 3a represents the OH2 interaction energies contoured at the  $-2.6$  kcal/mol level, from the template molecule **1**. It is obvious that hydrogen-bonding possibilities are present around the amide group and both of the nitrogens from the piperazine moiety. From this figure we also concluded that the OH2 probe is capable of reflecting the hydrogen-bonding properties of the ligands.

The CA+2 probe mimics the electrostatic interactions, and in Figure 3b we clearly see that real electrostatic fields are generated around the benzamide part of the template molecule **1** on the  $-3$  kcal/mol level. Finally, the field generated by the C3 probe (Figure 3c) on the  $0.02$  kcal/mol level indicates the smallest distance a noncharged molecule may approach the template without causing repulsive interactions. The energy cutoffs,

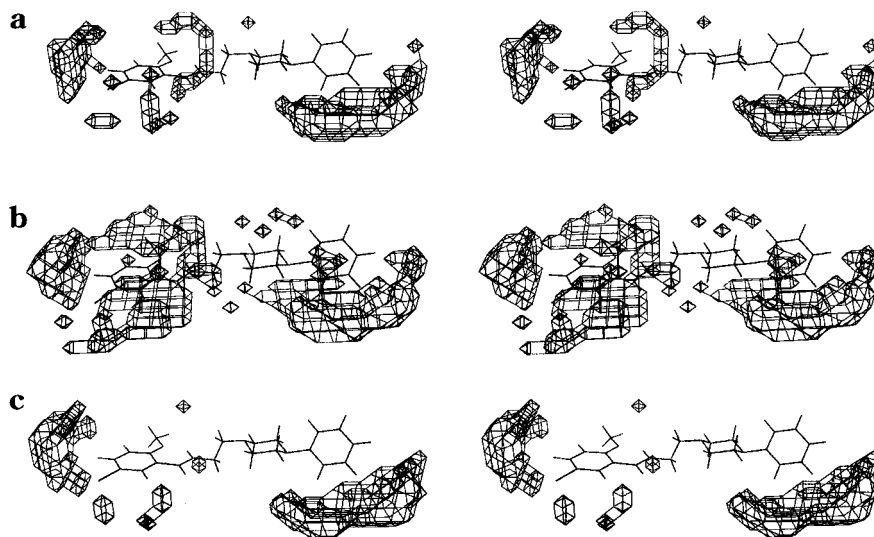


**Figure 4.** Each ligand is represented by three grids, one from each probe, and in order to perform multivariate analyses the grids were unfolded to form a row. The total data set, including unfolded interaction values from all ligands, was collected in a  $30 \times 25110$  matrix.

used above, have no relative relevance but were chosen in order to clearly describe the different fields.

In the final model each ligand was represented by its interactions with the three selected probes, unfolded to form a row, leaving a final  $30 \times 25110$  matrix (Figure 4). Worth mentioning is that the standard deviation in grid points close to substituent groups present in all ligands is very low (Figure 5). For instance, the strong hydrogen-bonding field present around the amide part of the template molecule **1** in Figure 3a is present in all ligands, and consequently, the standard deviation in this region becomes low as can also be seen in Figure 5a. PLS will focus on variables (grid points) with high standard deviations, and it may therefore turn out that important areas, as the amide part, get a too low weight in the final PLS solution. Therefore, it is important to study the individual fields from the ligands so that these interaction areas are not neglected or forgotten.

**Variable Pretreatment.** As explained earlier, GOLPE offers a lot of different pretreatment options and should be applied to best suit the data in question. Our data consist of 25 110 variables generated in GRID, 8370 from each of the three probes OH2, C3, and CA+2, respectively. The positive maximum cutoff was set to 5 kcal/mol already during the generation of the data in GRID. In order to correct for round off errors,<sup>5</sup> GOLPE automatically rejects columns (variables) having a total sum of squares (SS) lower than  $10^{-7}$ .



**Figure 5.** Contour maps of the standard deviations, all 30 compounds considered, from the OH2 (a), CA+2 (b), and C3 (c) probes. Only standard deviations higher than 2 are shown for clarity.

**Table 5.** Impact of Pretreatment, D-Optimal Variable Preselection, and FFD Variable Selection on the Fitted  $R^2$  and the Predicted  $Q^2$  (Cross-validation leave-one-out)

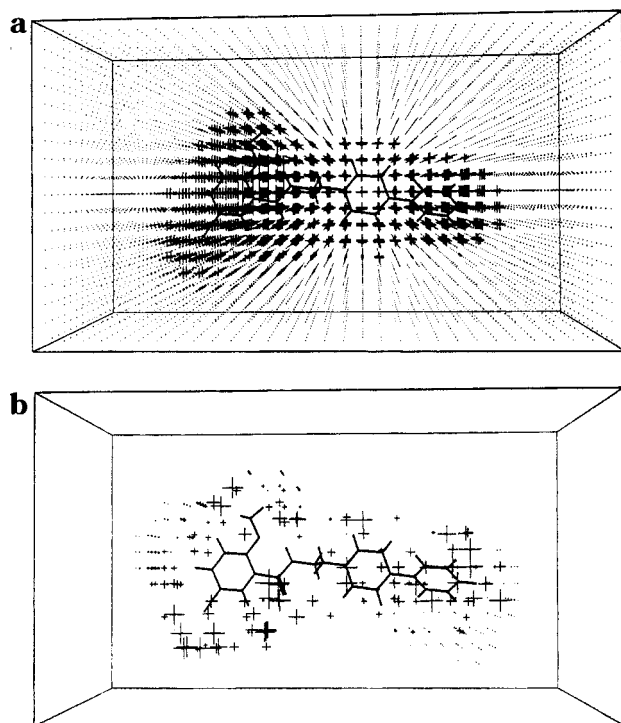
	no. of var	no. of compd <sup>a</sup>	$R^2$	$Q^2$
after pretreatment	19180	2	0.76	0.45
after D-opt selection	1192	3	0.85	0.49
after FFD <sup>b</sup> selection	784	2	0.80	0.65

<sup>a</sup>The number of components determined with leave-one-out cross-validation. <sup>b</sup>After the fractional factorial design selection.

Absolute values lower than 0.01 kcal/mol were set to zero, and as a consequence another 2000 variables were omitted from further modeling due to a too low variation ( $SS < 10^{-7}$ ). By introducing a lower limit for the standard deviation of the columns, the number of variables may be reduced significantly and render the absolute value cutoff almost useless.<sup>14</sup> We considered this action as a variable selection method in itself and chose not to utilize this option, and instead we put our trust in the GOLPE variable selection methodology.

Further, all 2-, 3-, and 4-level variables present were removed followed by a block-scaling procedure, as described in the theory part. The pretreatment procedure reduced the actual number of variables from 25 110 to 19 180, without any real variable selection.

**D-Optimal Variable Preselection.** The most informative variables are the ones spanning the space defined by the weight vectors as broadly as possible, under the constraint that a sufficient number of components are considered. If too few components are considered, information may be lost due to the fact that significant variables may not have been selected. The opposite is valid if too many components are considered, e.g., variables not correlated with the biological activity may be selected and introduce random variation in the model. Cross-validation<sup>24</sup> is the most commonly used method for determination of the proper dimensionality of a 3D QSAR model. However, at this early stage of modeling we are not interested in predictability but want to make sure a sufficient number of components is considered. A leave-one-out cross-validation experiment (not presented) gave the highest  $Q^2$  (0.45) after two components (Table 5), and we chose to perform the D-optimal preselection procedure with three compo-



**Figure 6.** Actual field from the CA+2 probe where the value in each grid point is proportional to the size of the cross. The field from compound **1** is pictured (a) before pretreatment and (b) after pretreatment and variable selection.

nents, assuming three were enough to capture all the significant information hidden in the data.

Each time 50% of the variables were selected. Each selection was preceded by calculation of a new PLS model including only the last selected variables. The selection procedure was repeated four times before the  $R^2$  started to decrease, with a reduction of the number of variables from 19 180, 9543, 4771, 2385, to 1192, respectively.

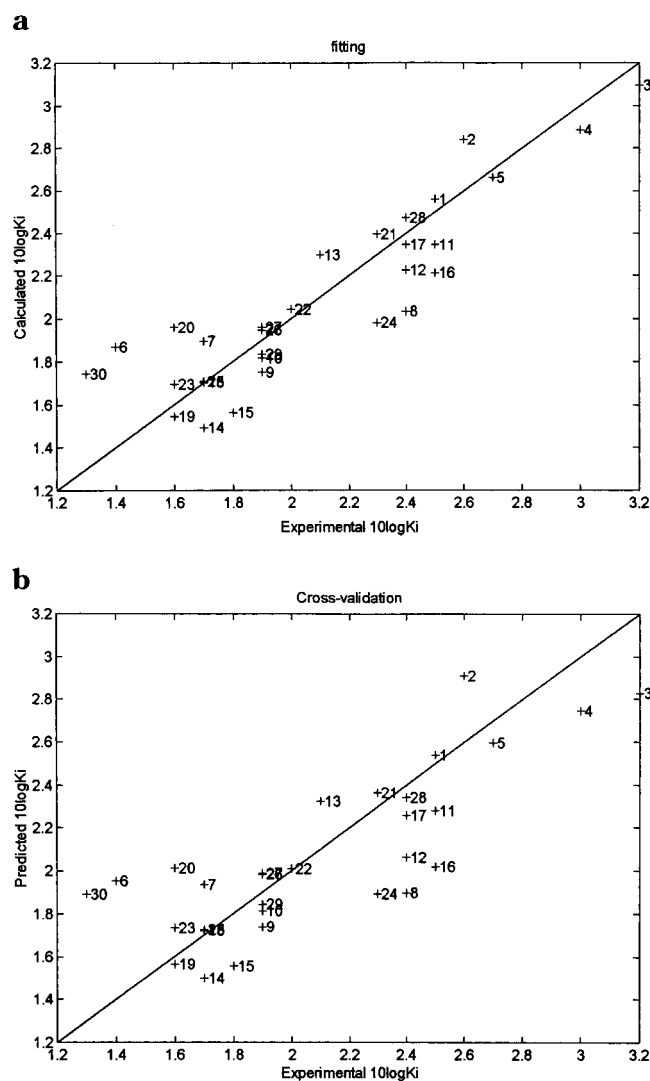
**Variable Selection.** The matrix containing only the 1192 variables left after the D-optimal preselection procedure was used as input for the final step in GOLPE. A design matrix with 4096 numbers of experiments (rows) and 299 numbers of dummy variables (theory part) was created, and each experiment was validated with cross-validation (five random groups repeated 20 times). The fractional factorial design procedure resulted in 313 and 408 variables with significant positive and significant negative effects on the predictability, respectively. Accordingly, 408 variables were omitted and 313 maintained together with 471 variables with nonsignificant effects on the predictivity, leaving 784 variables for the final model. Variables from a 3D QSAR study differ from classic chemometric variables in the sense that each variable represents a definite spatial coordinate in the grid. Therefore, it is also interesting to see where the selected variables are situated in the different fields. In Figure 6 the variables after pretreatment are compared with what remained after variable selection in the CA+2 field. Similar plots can be made for all fields.

Since we did not use an external test set, the final model was validated with cross-validation in three different ways (Table 6): first, with the leave-one-out procedure followed by leave-two-out, and finally, groups of five were left out and repeated 20 times.<sup>22</sup> The last

**Table 6.** Different Cross-Validation Experiments with the Final Model<sup>a</sup>

experiment	no. of compd <sup>a</sup>	$Q^2$
leave-one-out	2	0.65
leave-two-out	2	0.65
five random groups	2	0.63

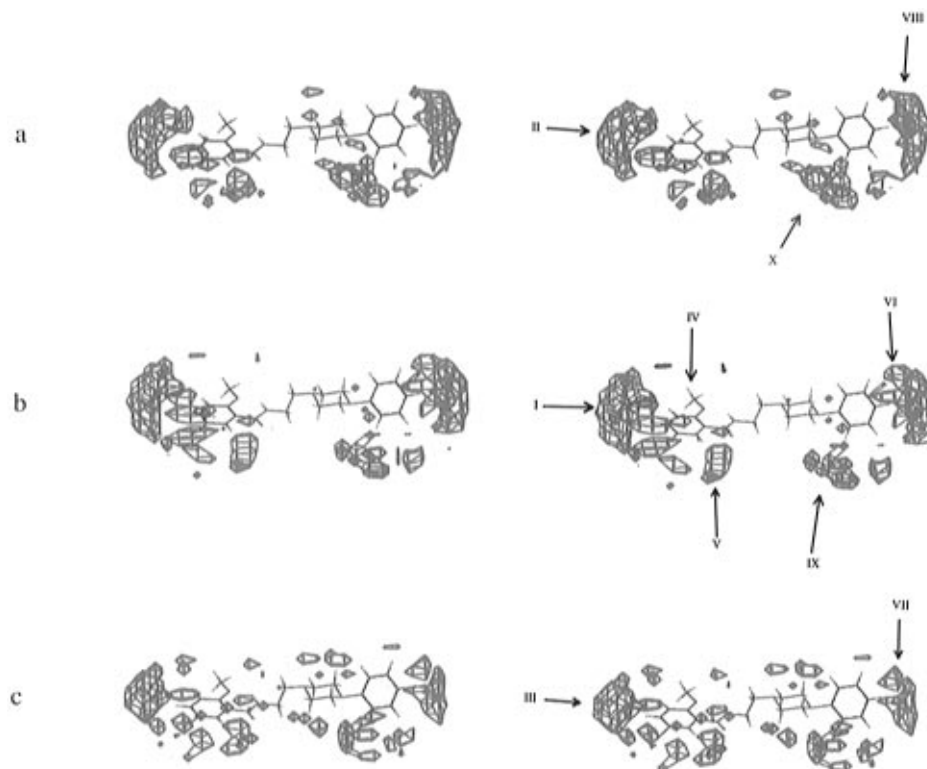
<sup>a</sup> For a more detailed description over the different experiments, refer to the text. <sup>b</sup> The number of components with maximum  $Q^2$ .



**Figure 7.** (a) Experimental  $^{10}\log K_i$  versus the calculated  $^{10}\log K_i$  from the second component in the final PLS model. (b) Experimental  $^{10}\log K_i$  versus the predicted  $^{10}\log K_i$  after leave-one-out cross-validation and two components.

validation experiment is a mixture between cross-validation and bootstrapping in the sense that each cross-validation experiment was repeated a number of times, as in bootstrapping, and the objects were included only once, as in cross-validation.

Two components were sufficient ( $R^2 = 0.80$ ) to explain most of the variation in  $^{10}\log K_i$ , and the correlation between the experimental  $^{10}\log K_i$  and the calculated  $^{10}\log K_i$  is plotted in Figure 7a. The GOLPE variable selection procedure has indeed improved the predictability of the model by increasing the cross-validated  $Q^2$  from 0.45 to 0.65 (Table 5). A  $Q^2$  of 0.65 is considered a good correlation between the experimental  $^{10}\log K_i$  and the predicted  $^{10}\log K_i$  as plotted in Figure 7b. In order to increase the interpretability of the PLS model, the weighted PLS coefficients from the second component



**Figure 8.** Contour maps of the PLS coefficients after the second component: (a) from the OH2 probe, (b) from the C3 probe, and (c) from the CA+2 probe. Only coefficients higher than  $|0.0005|$  are shown for clarity.

were plotted as contour plots connecting grid points with similar values (Figures 8). The negative and positive coefficient fields are blue and red, respectively. In order to simplify the interpretation of the figures, the following PLS equation (eq 5) (mean-centered model) is of good help. The  $b_j$  and the  $X_j$  are the PLS coefficients and the actual fields in each specific grid point ( $j$ ), respectively. The  $b_j$  values are the coefficients plotted in Figure 8.

$${}^{10}\log K_i = b_1 \times X_1 + b_2 \times X_2 + \dots + b_n \times X_n \quad (5)$$

In the design of new ligands the effects on the different fields in the regions where new substituents are placed are of importance. For instance, a substituent able to form hydrogen bonds will produce a negative OH2 field and must be placed in regions with positive PLS coefficients (red), in order to improve binding (decrease  ${}^{10}\log K_i$ ). The same reasoning is valid for all fields (Figure 8).

In the position para to the amide group of the benzamide moiety, there is space for substituents (Figure 8b, arrow I) unable to form hydrogen bonds (Figure 8a, arrow II) and which produce repulsive interactions with the CA+2 probe (Figure 8c, arrow III). This is the case with the additional phenyl ring present in the naphthamide ligands, which in general have lower  $K_i$  values than the benzamide ligands. The electrostatic field around the phenyl ring is negative above and under the ring, but the positive field close to the hydrogens appears to affect the  ${}^{10}\log K_i$  the most.

In one of the ortho positions (Figure 8b, arrow IV) a methoxy group is necessary in order to make an internal hydrogen bond interaction possible and fix the benzamide and the naphthamide moieties in a planar conformation. Accordingly, it can also be concluded from

the model that there is no room for substituents (Figure 8b, arrow V) in the second ortho position.

The phenyl ring in the phenylpiperazine tail may not be substituted in the para position (Figure 8b, arrow VI) due to steric reasons; however, an attractive interaction with the CA+2 probe (Figure 8c, arrow VII) promotes binding. Therefore, a small substituent with a negative electrostatic potential and with the ability to form hydrogen bonds<sup>25</sup> (Figure 8a, arrow VIII), like a fluorine atom, could be appropriate. The ortho position on the phenylpiperazine phenyl (Figure 8b, arrow IX) may very well be substituted, but substituents able to form hydrogen bonds will not improve binding (Figure 8a, arrow X).

Additionally, an unsubstituted phenylpiperazine moiety seems to be less potent than a substituted one, and a speculative explanation therefore could be that an unsubstituted ligand in solution more often has a planar phenylpiperazine tail than what could be expected from X-ray structures. This, in turn, could sterically hinder the ligand to interact with the receptor where a more twisted conformation may be preferable, which always is the most likely conformation on an ortho-substituted ligand.

As explained in the theoretical, the hydrogen-bonding properties of the amide part and the basic nitrogen of the arylpiperazine tail are of significance and should definitely be taken into account if one, for instance, wishes to prepare a minireceptor model<sup>26</sup> with this study as a reference.

## Conclusions

We have obtained a 3D QSAR model from a series of 30 compounds. The ligands were described quantitatively with GRID parameters, and the model was optimized by selecting only the most informative vari-

ables with the GOLPE algorithm, e.g., reduction of the number of variables from 25 110 to 784. As the number of variables was reduced, the predictability ( $Q^2$ ) of the model increased, indicating the necessity of a thorough variable selection procedure, also found by others.<sup>7,27</sup> The final model had a  $Q^2$  of 0.65, which can be considered sufficient for a 3D QSAR model. We also stress the importance of not focusing only on the  $Q^2$  when validating a 3D QSAR model but also studying the grid plots of the PLS coefficients in combination with the actual field plots. This is necessary in order to find out whether the model makes sense or not. It seems as if we have obtained a reasonable model, both regarding the predictability ( $Q^2$ ) and the graphic reliability (grid plot).

This model has been validated only internally, but in future work we intend to investigate the predictive ability also externally (test set) and with other regression methods.<sup>28</sup> Recently, Bro et al.<sup>29</sup> published the multiway PLS (N-PLS) algorithm, and by applying this regression method on 3D QSAR data, improvements in the interpretation and the predictability are expected.<sup>28</sup> Additionally, the N-PLS algorithm can also be used as an alternative variable selection method with a significant reduction in computer time as a result.

**Acknowledgment.** We are grateful for financial support from Dr. Saal van Zwanenbergstichting.

## References

- (1) Sautel, F.; Griffon, N. A Functional Test identifies Dopamine Agonists Selective for D3 versus D2 Receptors. *NeuroReport* **1995**, *6*, 329–32.
- (2) Glase, S.; Akunne, H. C.; Heffner, T. G.; Johnson, S. J.; Kesten, S. R.; MacKenzie, R. G.; Manley, P. J.; Pugsley, T. A.; Wright, J. L.; Wise, L. D. 4-Bromo-1-Methoxy-N-[2-(4-aryl-1-piperazinyl)-ethyl]-2-Naphthalenecarboxamides: Selective Dopamine D3 Receptor Partial Agonists. *Bioorg. Med. Chem. Lett.* **1996**, *6*, 1361–6.
- (3) SYBYL, Molecular Modeling Software, version 6.2; Tripos Inc., **1995**.
- (4) Cramer, R. D., III; Patterson, D. E.; Bunce, J. D. Comparative Molecular Field Analyses (CoMFA). 1. Effect of Shape on Binding of Steroids to Carrier Proteins. *J. Am. Chem. Soc.* **1988**, *110*, 5959–67.
- (5) Clementi, S. GOLPE 3.0; Multivariate Infometric Analyses (MIA): Perugia, Italy, 1995; SGI.
- (6) Goodford, P. GRID Molecular Discovery Ltd.: Oxford, England, 1995; SGI.
- (7) Cruciani, G.; Watson, K. A. Comparative molecular field analysis using GRID force-field and GOLPE variable selection methods in a study of inhibitors of glycogen phosphorylase b. *J. Med. Chem.* **1994**, *37*, 2589–601.
- (8) Geladi, P.; Kowalski, B. R. Partial Least Squares: A Tutorial. *Anal. Chem. Acta* **1986**, *185*, 1–17.

- (9) Jöreskog, K.; Wold, H., Eds. *Chemical Systems under Indirect Observation*; North Holland: Amsterdam, 1982; 191 pages.
- (10) Wold, S. Cross-validated Estimation of the Number of Components in Factor and Principal Components Models. *Technometrics* **1978**, *20*, 397–405.
- (11) Cruciani, G.; Baroni, M.; Costantino, G.; Riganelli, D.; Skagerberg, B. Predictive Ability of Regression Models. Part 1: Standard Deviation of Prediction Errors (SDEP). *J. Chemom.* **1992**, *6*, 335–46.
- (12) Mitchell, T. J. An Algorithm for the Construction of "D-optimal" Experimental Designs. *Technometrics* **1974**, *16*, 203–10.
- (13) Steinberg, D. M.; Hunter, W. G. Experimental Design Review and Comment. *Technometrics* **1984**, *26*, 71–6.
- (14) Baroni, M.; Costantino, G.; Cruciani, G.; Riganelli, D.; Valigi, R.; Clementi, S. Generating Optimal Linear PLS Estimations (GOLPE): An Advanced Chemometric Tool for Handling 3D-QSAR Problems. *Quant. Struct.-Act. Relat.* **1993**, *12*, 9–20.
- (15) Morgan, E. In *Chemometrics: Experimental Design*; Chadwick, N., Ed.; John Wiley and Sons Ltd.: Chichester, U.K., **1991**.
- (16) Mohamadi, F.; Richards, N. G. J.; Guida, W. C.; Liskamp, R.; Lipton, M.; Caufield, C.; Chang, G.; Hendrickson, T.; Still, W. C. MacroModel-An integrated Software System for Modelling Organic and Bioorganic Molecules Using Molecular Mechanics. *J. Comput. Chem.* **1990**, *11*, 440–67.
- (17) Clark, M.; Cramer, R. D., III; Van Opdenbosch, N. Validation of the General Purpose Tripos 5.2 Force Field. *J. Comput. Chem.* **1989**, *10*, 982–1012.
- (18) APOLLO - Automated Pharmacophore Location through Ligand Overlap; Koehler KF, 1996; SGI.
- (19) Walters, P.; Stahl, M. Babel-fileconversion, 1.1; Dolata Research Group, 1994.
- (20) Van Vliet, L. A.; Tepper, P. G.; Dijkstra, D.; Damsma, G.; Wikström, H.; Pugsley, T.; Akunne, H. C.; Heffner, T. G.; Glase, S. A.; Wise, L. D. Affinity for Dopamine D2, D3 and D4 Receptors of 2-Aminotetralins. Relevance of D2 Agonist Binding for Determination of Receptor Subtype Selectivity. *J. Med. Chem.* **1996**, *39*, 4233–4237.
- (21) Cheng, Y.-C.; Prusoff, W. H. Relationship Between the Inhibition Constant (K<sub>i</sub>) and the Concentration of Inhibitor Which Causes 50% Inhibition (IC<sub>50</sub>) of an Enzymatic Reaction. *Biochem. Pharmacol.* **1973**, *22*, 3099–108.
- (22) Wold, S.; Albano, C.; Dunn, W. J., III; et al. Chemometrics mathematics and Statistics in Chemistry. In *Proceedings of the NATO Advanced Study on Chemometrics*; Kowalski, B. R., Ed.; D. Reidel Publishing Co.: Dordrecht, 1984; pp 1–79.
- (23) Goodford, P. Multivariate Characterization of Molecules for QSAR Analyses. *J. Chemom.* **1996**, *10*, 107–17.
- (24) Jones, G.; Willet, P.; Glen, R. C. A Genetic Algorithm for Flexible Molecular Overlay on Pharmacophore Elucidation. *J. Comput.-Aid. Mol. Des.* **1995**, *9*, 532–49.
- (25) March, J. In *Advanced Organic Chemistry: Reactions, Mechanisms and Structure*, 4th ed.; March, J., Ed.; John Wiley & Sons: New York, 1996; 75 pages.
- (26) YAK, 3.8-GL; SIAT Biographics Laboratory, 1996.
- (27) Baroni, M.; Clementi, S.; Cruciani, G.; Costantino, G.; Riganelli, D.; Oberrauch, E. Predictive Ability of Regression Models. Part II: Selection of the Best Predictive PLS Model. *J. Chemom.* **1992**, *6*, 347–56.
- (28) Nilsson, J.; Wikström, H.; Smilde, A. Multiway Calibration in 3D QSAR. Part 1: Calibration and Validation. Internal Report, Department of Medicinal Chemistry, Rijksuniversiteit Groningen, The Netherlands, 1996.
- (29) Bro, R. Multiway Calibration. Multilinear PLS. *J. Chemom.* **1996**, *10*, 47–61.

JM9605952